SUPPLEMENTAL INFORMATION

Results

The aromatic finger mutation (AFM) does not affect secondary structure content – Secondary structure content estimated by analysis of CD spectra for the MBP-BECN1 CCD-BARAD and the MBP-BECN1 CCD-BARAD^{AFM} indicates that the AFM does not change the secondary structure content of the BECN1 CCD-BARAD (Fig. S3, Table S1), regardless of the presence of the tetrad mutation (data not shown). The MBP-BECN1 CCD-BARAD contains 269 helical, 82 strand, and 296 coil residues while the MBP-BECN1 CCD-BARAD^{AFM} contains 263 helical, 89 strand, and 299 coil residues (Table S1). Since for each class of secondary structure, secondary structure content does not vary beyond 10% between MBP-BECN1 CCD-BARAD and MBP-BECN1 CCD-BARAD^{AFM}, we conclude the AFM does not alter the secondary structure of these proteins.

The AFM does not affect the tertiary structure in solution – SEC-SAXS were recorded for the MBP-BECN1 CCD-BARAD (Fig. S4A) and MBP-BECN1 CCD-BARAD^{AFM} proteins (Fig. S4E). An R_g of 71 Å (Table S2) is estimated from the Guinier plots and P(r) plots of MBP-BECN1 CCD-BARAD (Fig. S4B and C), as well as MBP-BECN1 CCD-BARAD^{AFM} (Fig. S4F and G). Similarly, a D_{max} of 250 Å is estimated from the P(r) distribution for both samples (Fig. S3C and G; Table S2). Further, the the P(r) plots (Fig. S4C and G) and Kratky plots (Fig. S4D and H) indicate that both the MBP-BECN1 CCD-BARAD and MBP-BECN1 CCD-BARAD^{AFM} are well folded. The P(r) plots (Fig. S4C and G) also suggest a dumbbell shaped envelope for both samples. This similarity in size and shape of the WT and AFM mutant MBP-BECN1 CCD-BARAD indicates that the tertiary structure of the BARAD is unaffected by the AFM.

Experimental procedures

Plasmid preparation and protein expression – The human BECN1 CCD-BARAD (residues 175-450) was cloned between the NcoI and NotI restriction enzyme sites of the pMBP-Parallel-1 expression vector. The long, flexible linker between the MBP-tag and N-terminus of the BECN1 domains was replaced with a short, triple alanine linker via site-directed mutagenesis (primer: 5' GCC CTG AAA GAC GCG CAG ACT AAT GCA GCA GCA CTG TAT TTT CAG GGC GCC 3'). *E. coli* Arctic Express cells were transformed by the WT and AFM MBP-SL-BECN1-CCD-BARAD expression vectors and grown in LB medium with 100 µg/mL ampicillin at 30 °C to an A_{600} of ~0.6 prior to allowing the temperature to equilibrate to 10 °C. Recombinant protein expression was then induced by addition of 0.3 mM IPTG upon an A_{600} of 1.0-1.2 and expressed overnight.

Protein purification – For WT and mutant MBP-BECN1-CCD-BARAD constructs, fusion protein was purified from clarified crude cell lysate by amylose affinity chromatography (Wash buffer: 25 mM Tris-HCl pH 8.0, 300 mM NaCl, 10% v/v glycerol, 1 mM EDTA, 2 mM DTT) and eluted with wash buffer plus 20 mM maltose. Subsequently, the WT protein was loaded onto a 5/50 GL MonoQ (Pharmacia Biotech - GE Life Sciences, Pittsburgh, US) at 50 mM NaCl and eluted at 300 mM NaCl, which concentrated the protein to 7mg/mL. The amylose affinity elutions of the mutant BECN1-CCD-BARAD constructs were concentrated to 10mg/mL in a 50 kD Amicon Ultra-0.5 centrifugal concentrator (EMD Millipore, Billerica, MA, US). The proteins were purified to homogeneity by size exclusion chromatography (SEC), using a 16/60 Superdex 200 or 10/30 Superdex 200 (GE Life Sciences, Pittsburgh, PA, US) column (SEC buffer: 25 mM Tris-HCl pH 8.0, 300 mM NaCl, 2 mM DTT) and concentrated to 5 mg/mL in a 50 kD Amicon Ultra-0.5 centrifugal concentrator (EMD Millipore, Billerica, MA, US). At each stage of purification, protein purity was evaluated by SDS-PAGE stained with Coomassie Blue. In each case, the final purified protein was estimated to be >90% pure by Coomassie Blue stained SDS-PAGE.

SAXS data collection and analysis – SAXS data were recorded at the BioCAT beamline (ID18) (Advanced Photon Source, Argonne, IL, US) on a Pilatus 1M detector at a sample to detector distance of 3.5 m at a wavelength of 1.03 Å. For all constructs, SEC was performed in tandem with SAXS data collection to ensure that all SAXS data were collected from a homogenous sample eluting from the SEC column (Superdex 200 Increase 10/300 GL). SAXS data were recorded by exposing the column eluate to the X-ray beam for 1 second with a periodicity of 3 seconds. Scattering data were normalized to the incident X-ray beam intensity and scattering from buffer was subtracted prior to analysis using Igor Pro macros (1). Data was analyzed with the ATSAS program suite (2), including PRIMUS (3) to estimate Guinier extrapolations to calculate the radius of gyration (R_g) and Kratky plots to evaluate disorder within the samples. The P(r) function was plotted from the Fourier inversion of the scattering intensity, I(q) with GNOM (4) to estimate the R_g and maximum particle size (D_{max}).

CD spectroscopy – Continuous scanning CD spectra were recorded from 190 to 240 nm at 4 °C in a 300 μL quartz cell (0.1 cm path length) on a Jasco J-815 spectropolarimeter equipped with a Peltier thermoelectric temperature control for the WT or mutant MBP-SL-BECN1(175-450) protein at concentrations of 2-6 μM in 5 mM Na phosphate dibasic, 5mM Na phosphate monobasic pH 7.4, 100 mM $(NH_4)_2SO_4$. Secondary structure content was estimated by analyzing the CD data using the SDP48 reference protein database and three analysis programs, SELCON3, CDSSTR, and CONTIN, from the CDpro suite within the Jasco software (5-7). For each spectrum, the estimated secondary structure content obtained from the three CD data analysis programs was averaged and reported.

Tables

Table S1. Average estimated secondary structure content in MBP-BECN1-CCD-BARAD proteins.

Protein	# Residues	Helix (%)	Beta (%)	Coil (%)
MBP-BECN1(175-450)	651	41.3 ± 2.9	12.6 ± 1.0	45.5 ± 1.6
MBP-BECN1(175-450)^{AFM}	651	40.5 ± 1.3	13.7 ± 0.9	46.0 ± 0.9

Table S2. Summary of SEC-SAXS for MBP-BECN1-CCD-BARAD proteins.

Protein	MW_T (KD)	Guinier	P(r)	
		R_g (Å)	R_g (Å)	D_{max} (Å)
MBP-BECN1(175-450)	147.2 (dimer)	66	71	250
MBP-BECN1(175-450)^{AFM}	146.9 (dimer)	63	71	250

Table S3. Final protein constructs used in this study.

Label	Description	BECN1 Residues
BECN1 CCD	BECN1 CCD	175-265
BECN1 CCD^{TETRAD}	BECN1 CCD OH Tetrad Mutant	175-265, (V250A,M254A,L261A,L264A)
BECN1 OH+BARAD^{AFM}	His_6-BECN1 OH+BARAD Aromatic Finger Mutant	248-450, (F359D,F360D,W361D)
BECN1 OH+BARAD$^{AFM, TETRAD}$	His_6-BECN1 OH+BARAD Aromatic Finger Mutant + OH Tetrad Mutant	241-450, (F359D,F360D,W361D), (V250A,M254A,L261A,L264A)
BECN1 CCD-BARAD^{AFM}	BECN1 CCD-BARAD Aromatic Finger Mutant	175-450, (F359D,F360D,W361D)
BECN1 CCD-BARAD^{AFM,TETRAD}	BECN1 CCD-BARAD Aromatic Finger Mutant + OH Tetrad Mutant	175-450, (F359D,F360D,W361D), (V250A,M254A,L261A,L264A)

Figures

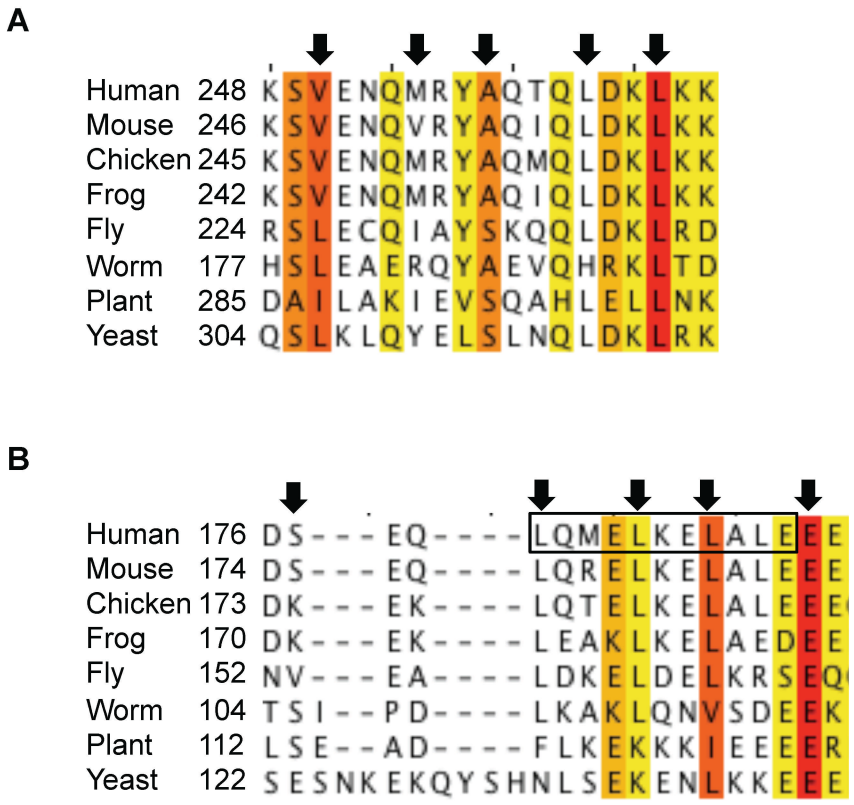

Figure S1. Sequence alignment of the overlap helix and partner helix in BECN1 orthologs. Increasing background color intensity corresponds to increasing residue conservation: with red corresponding to invariant residues of the A) Overlap helix and B) Partner helix with NES boxed. Interface residues are indicated with black arrows.

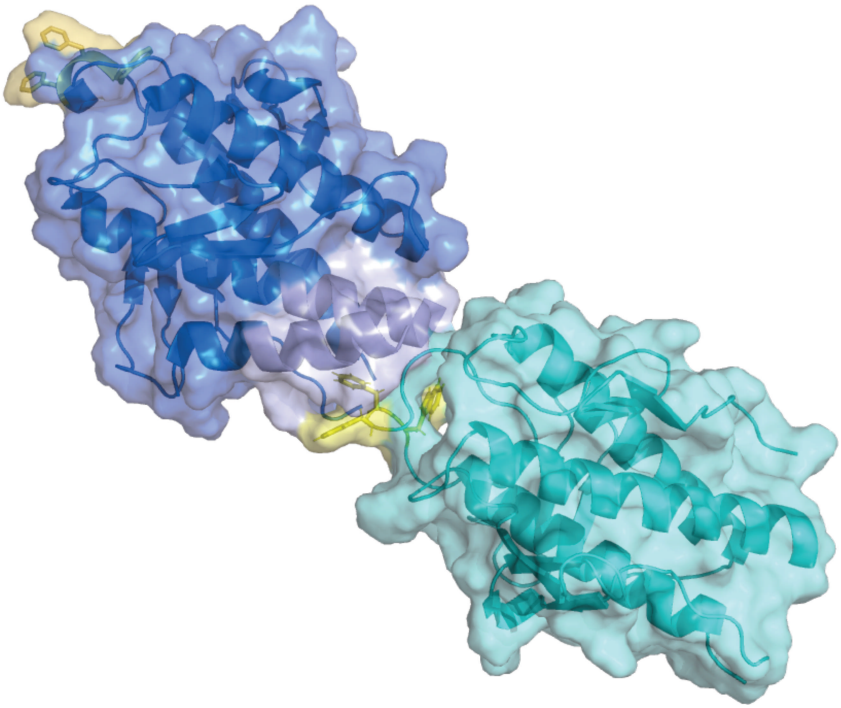

Figure S2. The aromatic finger of the OH+BARAD buried in the hydrophobic pocket of another molecule. The aromatic finger is shown in yellow and hydrophobic pocket is shown in grey.

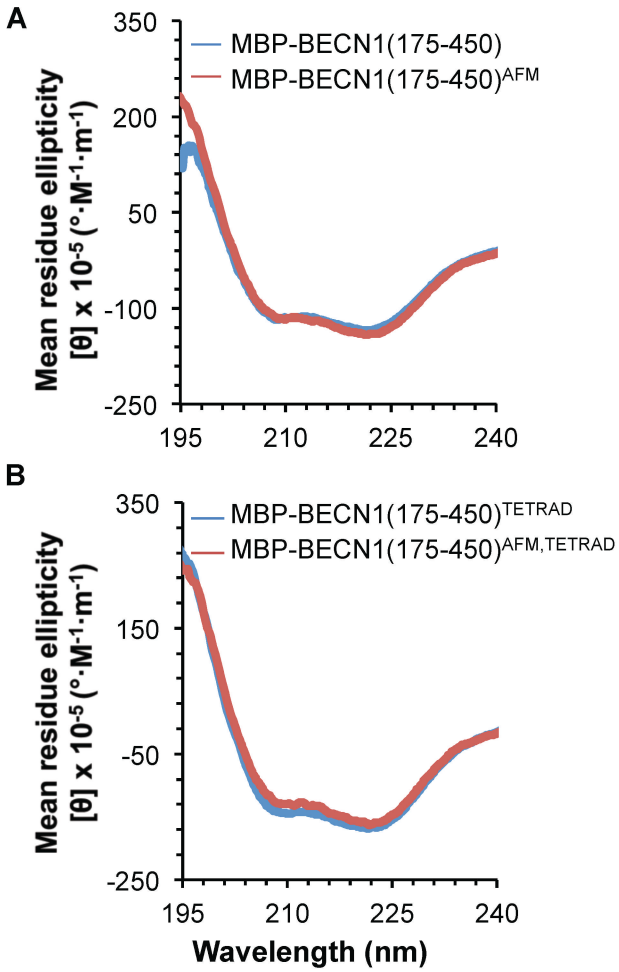

Figure S3. The AFM does not alter CD spectra of MBP-BECN1(CCD-BARAD). A) MBP-BECN1(175-450) and B) MBP-BECN1(175-450)^{TETRAD}.

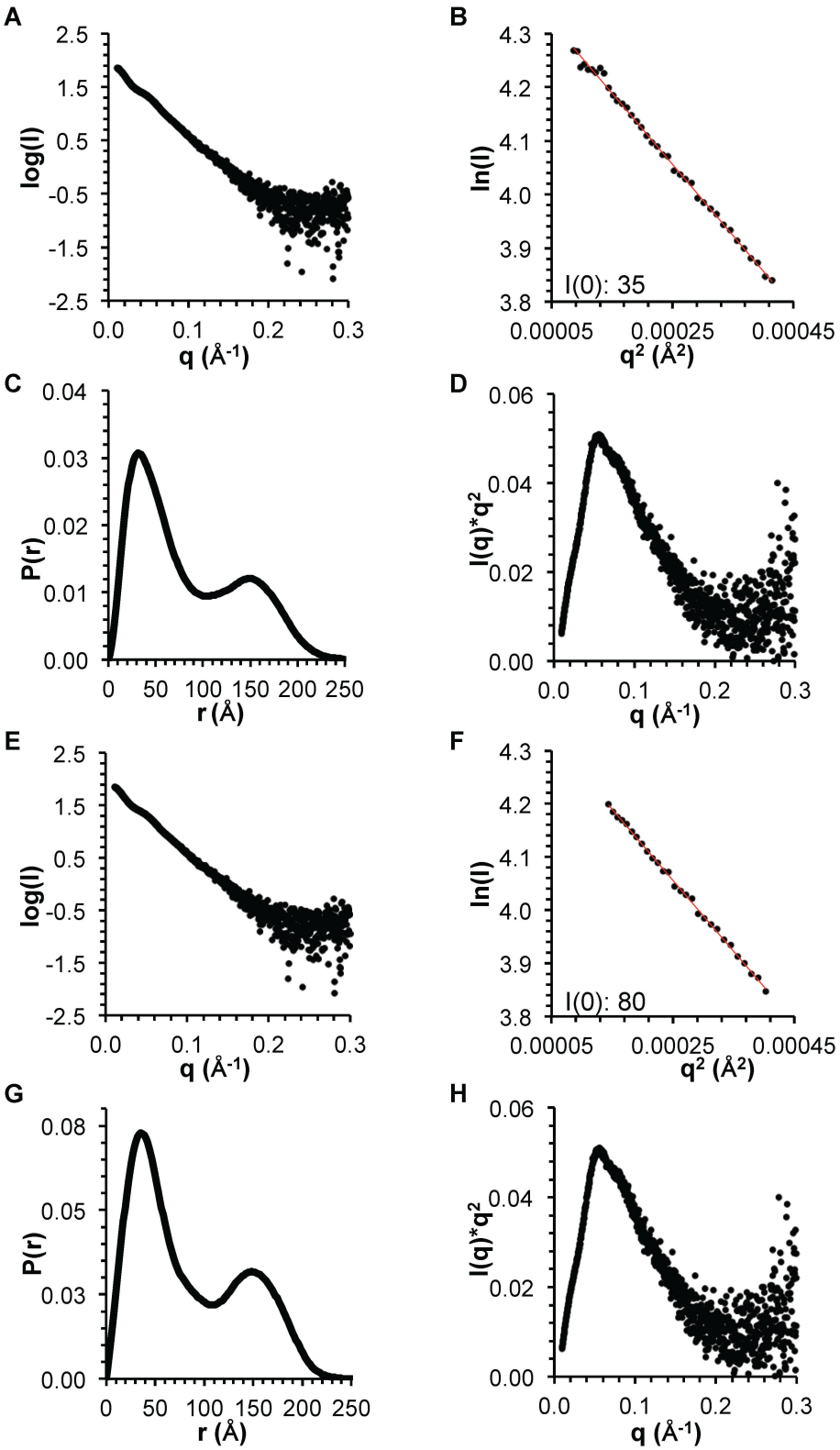

Figure S4. SEC-SAXS analysis of MBP-BECN1(CCD-BARAD) proteins. For the MBP-BECN1(CCD-BARAD), the A) scattering data, B) Guinier, C) P(r) pairwise distribution, and D) Kratky. For the MBP-BECN1(CCD-BARAD)^{AFM}, the E) scattering data, F) Guinier, G) P(r) pairwise distribution, and H) Kratky.

REFERENCES

1. Ilavsky, J., and Jemian, P. R. (2009) Irena: tool suite for modeling and analysis of small-angle scattering. *Journal of Applied Crystallography* 42, 347-353
2. Petoukhov, M. V., Franke, D., Shkumatov, A. V., Tria, G., Kikhney, A. G., Gajda, M., Gorba, C., Mertens, H. D. T., Konarev, P. V., and Svergun, D. I. (2012) New developments in the ATSAS program package for small-angle scattering data analysis. *Journal of Applied Crystallography* 45, 342-350
3. Konarev, P. V., Volkov, V. V., Sokolova, A. V., Koch, M. H. J., and Svergun, D. I. (2003) PRIMUS: a Windows PC-based system for small-angle scattering data analysis. *Journal of Applied Crystallography* 36, 1277-1282
4. Svergun, D. I. (1992) Determination of the regularization parameter in indirect-transform methods using perceptual criteria. *Journal of Applied Crystallography* 25, 495-503
5. Sreerama, N., Venyaminov, S., and Woody, R. (2000) Estimation of protein secondary structure from circular dichroism spectra: Inclusion of denatured proteins with native proteins in the analysis. *Analytical Biochemistry* 287, 243-251
6. Sreerama, N., and Woody, R. W. (2000) Estimation of protein secondary structure from circular dichroism spectra: comparison of CONTIN, SELCON, and CDSSTR methods with an expanded reference set. *Analytical Biochemistry* 287, 252–260
7. Sreerama, N., Venyaminov, S. Y., and Woody, R. W. (2001) Analysis of protein circular dichroism spectra based on the tertiary structure classification. *Analytical biochemistry* 299, 271-274